JREE: Vol. 9, No. 1, (Winter 2022) 63-69

Journal of Renewable Energy and Environment

Journal Homepage: www.jree.ir

Materials and Energy Research Center

MERC

Research Article

Surface Modification of Copper Current Collector to Improve the Mechanical and Electrochemical Properties of Graphite Anode in Lithium-Ion Battery

Mohsen Babaiee*, Mohammad Zarei-Jelyani*, Shaghayegh Baktashian, Rahim Eqra

Department of Energy Storage, Institute of Mechanics, Shiraz, Iran.

PAPER INFO

Paper history:
Received: 20 June 2021
Revised in revised form: 17 August 2021
Scientific Accepted: 30 August 2021
Published: 05 December 2021

Keywords:
Li-Ion Battery,
Current Collector,
Surface Modification,
Cu Foil,
Graphite

ABSTRACT

A mechanical technique was applied to the copper current collector of lithium-ion battery anode to improve interface adhesion between Cu foil and anode film. The mechanical and electrochemical performances of graphite anodes coated on Bare Cu Foil (BCF) and Modified Cu Foil (MCF) were evaluated. The BCF and MCF anodes exhibited adhesion strengths of 1.552 and 1.617 MPa, respectively. The electrochemical studies of BCF and MCF anodes showed that the initial discharge capacity of graphite anode coated on the MCF (323.6 mAh g^{-1}) was about 8 % higher than the BCF anode (299.9 mAh g^{-1}). The BCF anode capacity reached 227.9 mAh g^{-1} after 100 charge/discharge cycles at 0.5C rate, while this value was 247.7 mAh g^{-1} for MCF anode. The results of electrochemical impedance spectra demonstrated that the diffusion coefficient of lithium-ion for MCF anode was about 56 % higher than that for BCF anode. On the other hand, the surface modification of the copper current collector reduced the charge transfer resistance of anode from 28.5 Ω to 23.2 Ω.

https://doi.org/10.30501/jree.2021.290435.1219

1. INTRODUCTION

Given that the essential requirement of an eco-friendly energy including regulations on CO_2 emission and fossil fuel reduction is increasing, many studies are being carried out worldwide to develop high-performance energy storage systems [1, 2]. Recently, storage of electrical energy remains critically dependent on Lithium-Ion Batteries (LIBs). Therefore, advanced LIBs are required to address the increasing demand for energy sources with high capacities, which present high energy density, high power density, and better cycle stability than existing LIBs [3-7]. At present, the development of new materials for cathode, anode, membrane, and electrolyte are the most attractive approaches to improving the performance of LIBs [8-10]. Numerous researches have attempted to evaluate new electrode materials [11-13] and high-performance membranes and electrolytes [14, 15]. Some studies have also considered degradation mechanisms such as structural volume changes of active electrode material during lithiation and delithiation processes [16, 17].

However, the factors that affect LIB performance are limited to electrode materials, membranes, and electrolytes. As a critical component in LIBs, the current collector enhances battery performance significantly [18, 19]. The current collector not only acts as a bed for loading active materials, but also is responsible for collecting the electrical current produced by the electrode active materials and conducting it to the output. Unlike other battery components, current collectors, especially copper foils, have received insignificant attention, while they have a crucial impact on lithium-ion battery performance. In a conventional anode electrode of LIB, the surface of the copper foil is coated with graphite slurry. Bond strength, contact impedance of graphite/copper foil interface, and chemical and electrochemical stability are the significant factors impacting cycling stability and capacity of a lithium-ion battery [20, 21].

Mechanical damage to current collector foils in LIBs can lead to external electronic failure followed by battery failure [22]. Furthermore, it has been shown that the organic electrolyte of LIBs gradually etches the copper current collector [23], leading to the degradation of battery performance during long charge/discharge processes. In addition, in the case of traditional copper foils, the smooth surface of copper foil may cause poor contact with the graphite. This can cause high impedance in the contact interface as well as high risk of chemical corrosion in case of electrolyte exposure [24, 25].

Kang et al. synthesized a thin uniform and Compact Oxide Layer (COL) on an Al current collector for LIB cathode through the oxidation process using KMnO4 as an oxidant. They found that the COL on an Al current collector could

*Corresponding Author's Email: babaiee.mohsen@gmail.com (M. Babaiee); m.zarei@isrc.ac.ir (M. Zarei-Jelyani)
URL: https://www.jree.ir/article_141272.html

Please cite this article as: Babaiee, M., Zarei-Jelyani, M., Baktashian, Sh. and Eqra, R., "Surface modification of copper current collector to improve the mechanical and electrochemical properties of graphite anode in lithium-ion battery", ***Journal of Renewable Energy and Environment (JREE)***, Vol. 9, No. 1, (2022), 63-69. (https://doi.org/10.30501/jree.2021.290435.1219).

effectively protect it from corrosion and exhibit good adhesion properties and electrochemical performance for extensive cycle life [26].

Jeon et al. used two types of Cu foil, conventional flat Cu foil and rough Cu foil, to fabricate silicon (Si) electrodes for flexible and high-energy-density LIBs. When Cu foils with a roughness of 3 mm were used for the Si electrode, they delivered much better cycle performance, especially under lower binder content and in the mechanically stressed condition [27].

Jiang et al. synthesized a thin graphene film on the surface of Cu current collector by a large-scale Low-Pressure Chemical Vapor Deposition (LPCVD) process. Their modified Cu foil was used as a current collector to support spinel $Li_4Ti_5O_{12}$ anode directly. They represented that graphene coating Cu foil could effectively improve the overall Li storage performance of $Li_4Ti_5O_{12}$ anode [28].

Zhang et al. applied ultrafast laser ablation for the surface modification of Cu foil for preparation of artificial graphite anode films for LIBs. Improved adhesive force and electrochemical performance were confirmed in anode films on laser structured Cu foils [29].

In the present study, a mechanical abrasion method has been employed for the copper current collector (Figure 1) to increase its specific surface area and enhance mechanical performance. This surface treatment will increase the contact strength between the graphite active material and the current collector. Furthermore, the interface impedance is reduced and the corrosion resistance against the electrolyte increases using this surface modification method. Therefore, the surface treatment of copper foil improves the insertion/de-insertion process of lithium ions in/from the structure of graphite anode. This practical, simple and effective method can be applied to lithium-ion batteries with a long cycle life.

Figure 1. Schematic of current collector treatment and anode electrode preparation process

2. EXPERIMENTAL

2.1. Meterials

The active material for anode slurries was Mesocarbon Microbeads (MCMB, Gelon) with 16.5-19 µm mean diameter (d50), 1.28 g cm^{-3} tap density, and a specific surface area of less than 1.5 m^2 g^{-1}. The conductivity agent of Carbon black (CB, Super P Li, Gelon) with a density of 160 kg m^{-3} was used. A blend of carboxymethyl cellulose (CMC) and styrene-butadiene rubber (SBR) was utilized as the binder. The current collector of the electrode was Copper foil with a thickness of 9 µm.

2.2. Mechanical modification of current collector surface

The copper current collector was abraded using sandpaper (mesh 1000) to increase the roughness of the surface and the contact strength between the active material and the current collector. After mechanical treatment, the surface of copper foil was cleaned with acetone to prepare the current collector for coating of anode slurry. Figure 2 represents microscopic images of the surface of the copper foil before and after the abrasion process at 60 and 200x magnifications.

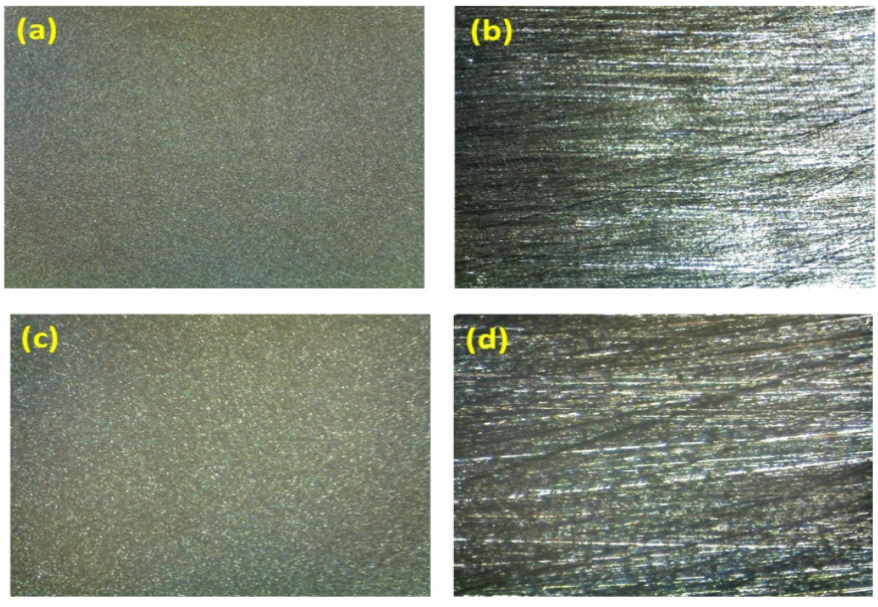

Figure 2. Microscopic images of the surface of the copper foil before abrasion process at: (a) 60x and (c) 200x magnifications and after abrasion process at (b) 60x and (d) 200x magnifications

2.3. Electrodes preparation

The composition of anode slurry coated on different current collectors is shown in Table 1. Active material (MCMB) and conductive agent (CB) were heated in a vacuum oven for 2 hours at 120 ºC to prepare the anode electrodes. A planetary mill was used for 30 minutes at a rate of 200 rpm in order to grind and mix the active and conductive materials. According to Table 1, the required amounts of CMC and SBR were mixed with distilled water and, then, were stirred for 24 h at ambient temperature. Afterward, the active material of the anode and conductivity agent were added to the binder solution. A vacuum-mixer was applied for degasing and further mixing of the blend at a rate of 200 rpm for 1.5 h. The homogenous prepared slurry was coated on bare Cu foil (BCF) and modified Cu foil (MCF) using a doctor-blade method. Then, the electrodes were dried overnight at 60 ºC and pressed using a roll press. This was to warrant good contact between the current collector and electrode mass, as well as between the electrode components. Figure 3 shows the SEM images of the anode electrodes with 1000 and 5000x magnifications.

Table 1. Composition of anode electrode components

Component	Composition (wt %)
Active material (MCMB)	94.5
Conductive agent (CB)	1
CMC	2.25
SBR	2.25

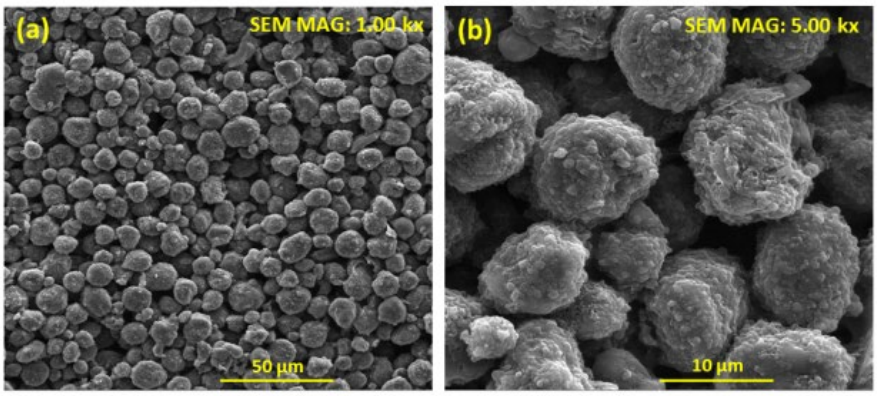

Figure 3. The SEM images of the anode electrodes with (a) 1000x and (b) 5000x magnifications

2.4. Cell assembly

The electrode sheets were punched to prepare the disks of the electrode with a diameter of 14 mm. Prior to assembly of a coin cell, the disks of the electrode were dried under vacuum at 60 ºC for 2 hours. The assembly of CR2032 coin-type half-cells was conducted in a glove box with oxygen and moisture levels lower than 0.5 ppm. The separator was a porous polymer film with a thickness of 25 µm. A solution of 1 M $LiPF_6$ in a mix of EC/DEC (1:1) (MTI Corporation) was utilized as an electrolyte. A foil of Li-metal with 0.6 mm thickness and 16 mm diameter (Gelon LIB Group) was employed as reference and counter electrodes. Finally, the sealing of cells was performed by an electric coin cell crimping machine (MTI Corporation). After assembly, the cells spent 3 hours in a resting state to ensure perfect electrolyte penetration through the pores of electrode and membrane.

2.5. Chraracterization

Quantification of the adhesion strength of anode coatings on the copper foil was conducted using a universal testing machine (Gotech). As shown in Figure 4, double-sided adhesive tape was used to fix an electrode disk between two parallel plates. A pre-compression load equal to 20 kg.f was applied to achieve a reproducible adhesive bond between compression grips and electrode. The disjunction speed of the grips was set at 5 mm/min. The value of the measured tensile stress was considered as adhesion strength.

Coin half-cells were charged and discharged by a battery tester (Neware technology ltd.) to evaluate the electrochemical performance at 0.5C rate in the range of 0.01-2.0 V. All electrochemical experiments were conducted at ambient temperature.

Electrochemical Impedance Spectroscopy (EIS) tests were performed under a frequency window of 10 mHz-100 kHz (open-circuit voltage was selected as the applied bias voltage). An equivalent electronic circuit was applied to simulate the experimental Nyquist plots using the NOVA software.

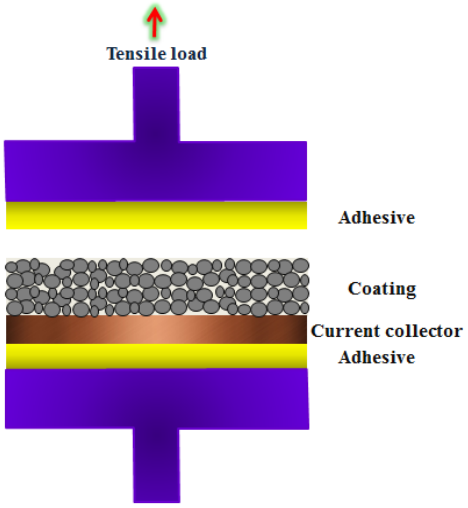

Figure 4. Mechanism of adhesion strength test

3. RESULTS AND DISCUSSION

Figure 5 shows the adhesion strength of MCMB anodes coated on Bare Cu Foil (BCF) and Modified Cu Foil (MCF). The BCF and MCF anodes exhibit adhesion strengths of 1.552 and 1.617 MPa, respectively. Therefore, the anode electrode

coated on the modified current collector has better adhesion properties, which can improve the mass loading of the electrode and increase the energy density of the LIB.

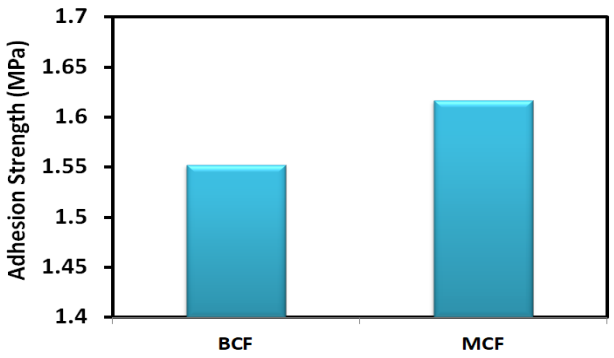

Figure 5. Adhesion strength of MCMB anodes coated on BCF and modified Cu foil (MCF)

Figure 6 represents the cycling performance of BCF and MCF anodes during 100 charge/discharge cycles at a rate of 0.5C. The initial discharge capacities of BCF and MCF anodes are 299.9 and 323.6 mAh g^{-1}, respectively. The modification of the surface of the current collector increases the initial discharge capacity of the MCMB anode by 7.9 %. In addition, the MCF anode capacity reaches 247.7 mAh g^{-1} after 100 cycles, while the BCF anode capacity is equal to 227.9 mAh g^{-1} in the 100th cycle. This means that after 100 cycles, the discharge capacity of the modified anode is 8.7 % higher than that of the BCF anode. On the other hand, the BCF anode has only passed 46 cycles to reach the capacity of 247.7 mAh g^{-1} (equal to the final capacity of the MCF anode after 100 cycles). This indicates that the cycle life of the modified anode is 2.2 times longer than that of the BCF anode to reach the capacity of 247.7 mAh g^{-1}. Figure 7 shows the discharge voltage profiles for BCF and MCF anodes at 1st, 20th, 40th, 60th, 80th, and 100th cycles. The electrochemical parameters of the voltage profiles are presented in Table 2.

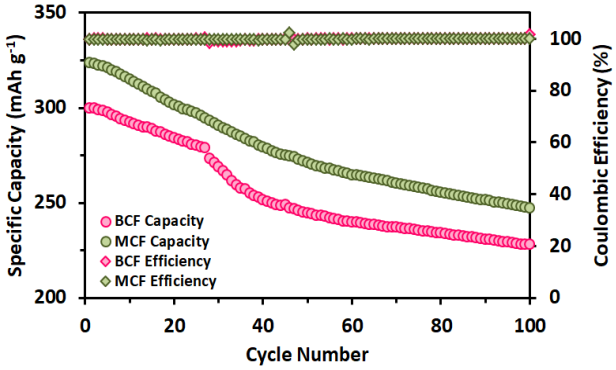

Figure 6. Cycling performance of BCF and MCF anodes during 100 charge/discharge cycles at 0.5C

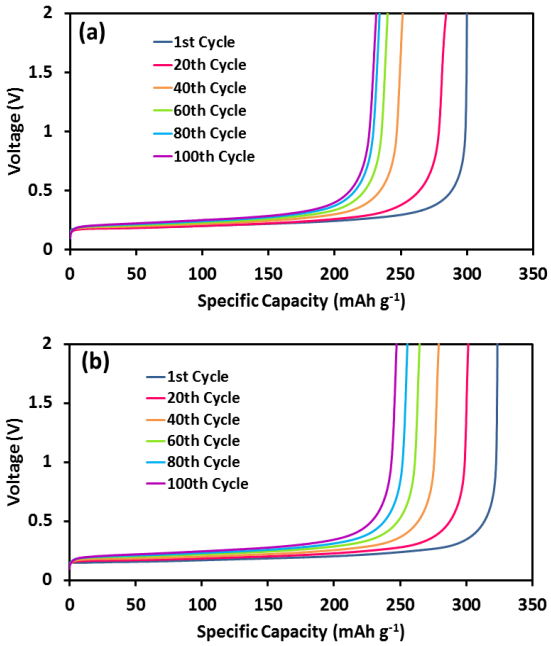

Figure 7. Discharge voltage profiles for BCF and MCF anodes at 1st, 20th, 40th, 60th, 80th, and 100th cycles

Table 2. The electrochemical parameters of the voltage profiles

Anode	Discharge capacity (mAh g^{-1})					
	1st cycle	20th cycle	40th cycle	60th cycle	80th cycle	100th cycle
BCF	299.9	284.2	251.2	240.1	234.0	227.9
MCF	323.6	301.6	279.2	264.2	255.5	247.7

Figure 8 demonstrates the differential capacity curves for anode half-cells of BCF (Figure 8a) and MCF (Figure 8b) in the discharge process of 20th, 40th, 60th, 80th, and 100th cycles. In these figures, two peaks are observed as the anode discharges from low voltage to high voltage, related to the delithiation process [30]. As shown in Figure 8a and b, the delithiation peaks are shifted to higher voltage during cycling, indicating that the resistance of anode half-cells increases as cycle number increases [31]. Figure 8c and d compares the differential capacity profiles of BCF and MCF anodes in the discharge process of 20th and 100th cycles, respectively. According to Figure 8c, it can be said that the average discharge voltage of the MCF anode is lower than that of BCF anode since the peak related to de-insrtion of lithium ions for the MCF anode occurs at lower voltages than that for BCF. Therefore, if the MCF and BCF anodes are employed in a full cell of LIB, the battery prepared by the MCF anode will have a higher discharge voltage. On the other hand, the higher peak intensity for the MCF anode points to the higher capacity of the MCF anode than that of the BCF anode.

Figure 9a displays the half-cells Nyquist plots of BCF and MCF anodes after 100 charge/discharge cycles. Each impedance spectrum shows two semicircles, simulated using an equivalent circuit (Figure 9a). The R_s shows the resistance of bulk electrolyte and high-frequency semicircle is considered the SEI film resistance (R_{SEI}). The observed semicircle at a medium frequency indicates the charge-transfer resistance (R_{ct}) of the lithiation process between the electrolyte and the electrode. CPE_{SEI} and CPE_{ct} elements are constant phase elements associated with R_{SEI} and R_{ct}, respectively. The low-frequency slope is attributed to Warburg impedance that represents the diffusion process of Li^+ ion in the electrode-electrolyte interface [32].

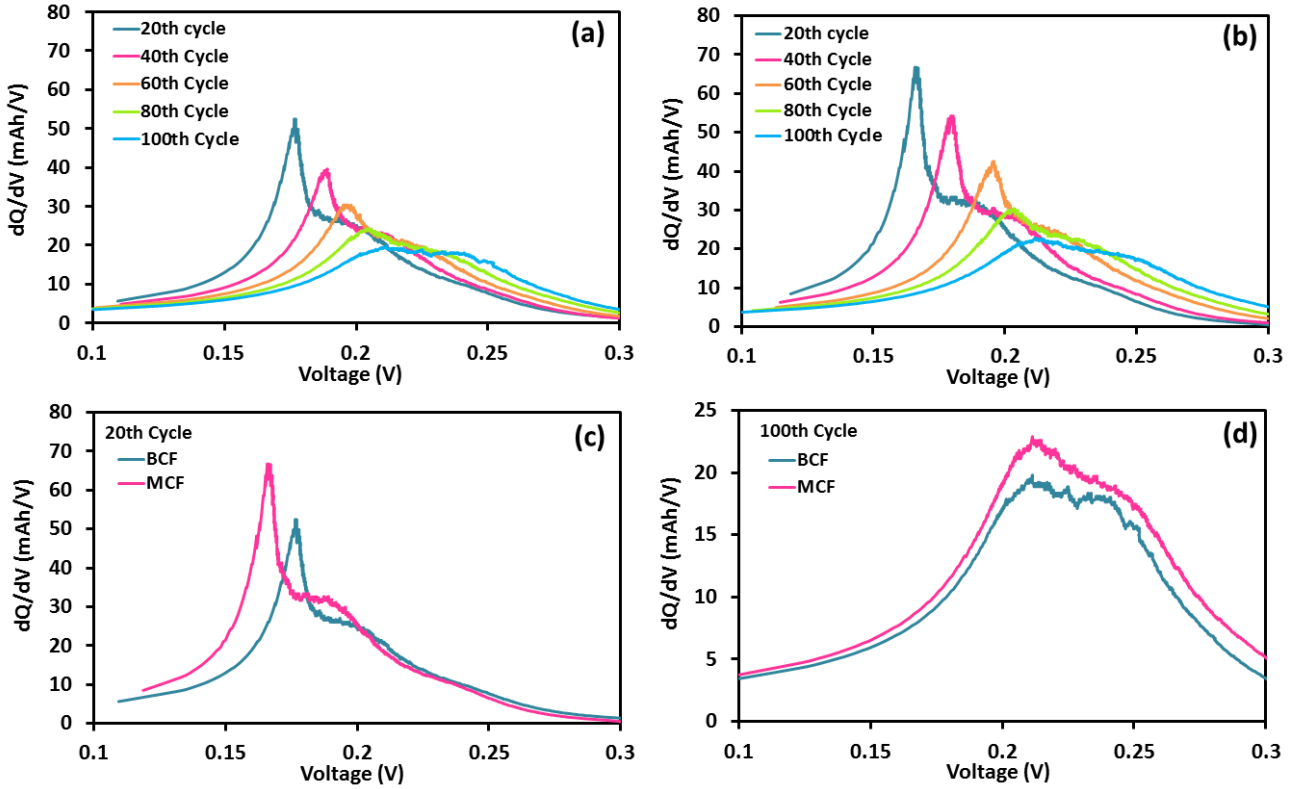

Figure 8. The differential capacity curves for anode half-cells of: (a) BCF, (b) MCF in the discharge processes of 20th, 40th, 60th, 80th, and 100th cycles; comparison of the differential capacity profiles of BCF and MCF anodes in the discharge process of (c) 20th cycle and (d) 100th cycle

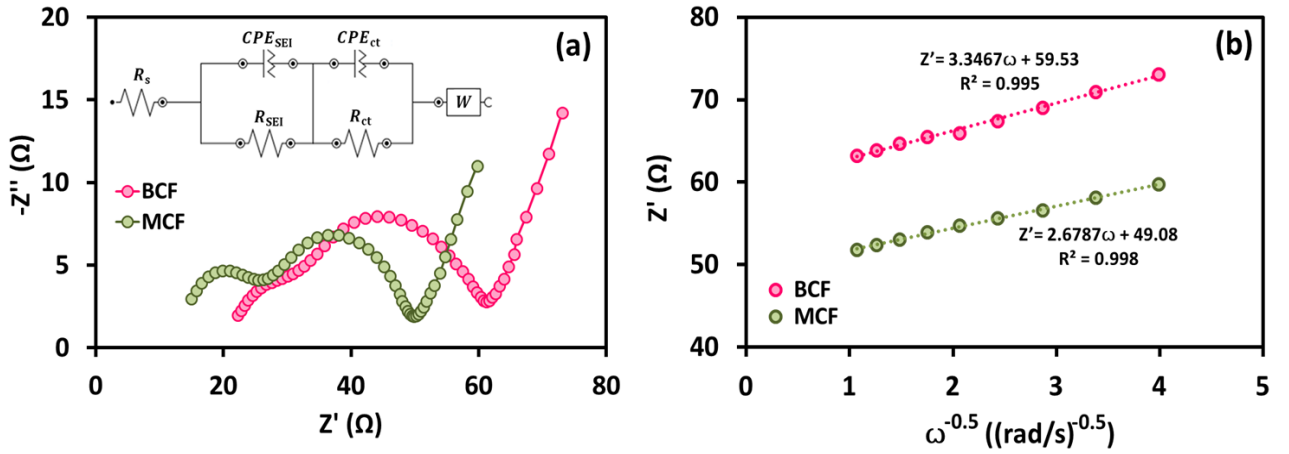

Figure 9. (a) The half-cells Nyquist plots of BCF and MCF anodes after 100 charge/discharge cycles at 0.5C; (b) diagram of the real part resistance with the inverse square root of the angular speed for the anodes of BCF and MCF (in the low-frequency region)

Table 3 presents the simulation results obtained from impedance spectrum of BCF and MCF anodes. The values of R_s are 20.1 Ω and 12.4 Ω for BCF and MCF electrodes, respectively. This indicates that the surface modification process of Cu foil has reduced the R_s by about 40 %. In addition, the MCF anode has lower charge-transfer resistance (23.2 Ω) than the BCF anode (28.5 Ω) after 100 cycles at a rate of 0.5C.

Figure 9b shows a diagram of the real part resistance with the inverse square root of the angular speed for the anodes of BCF and MCF (in the low-frequency region). In order to determine the Warburg factor (σ) and lithium diffusion coefficient (D_{Li^+}), Equations (1) and (2) were applied, respectively [33].

$$Z' = R_s + R_{SEI} + R_{ct} + \sigma\omega^{-0.5} \quad (1)$$

$$D_{Li^+} = \frac{R^2T^2}{2A^2n^2F^4C^2\sigma^2} \quad (2)$$

where the parameters are defined as follows:

Z′: real part resistance
ω: angular frequency
R: gas constant
T: absolute temperature
A: electrode surface area
F: Faraday constant
C: Li–ion molar concentration in an active material

According to Equation (1), the slope of the line obtained in Figure 9b represents the Warburg factor (σ), which is equal to 3.347 and 2.679 for the BCF and MCF anodes, respectively. Since all parameters of Equation (2) are the same for BCF and

MCF anodes except σ, the ratio of lithium diffusion coefficients is calculated using Equation (3).

$$\frac{D_{Li^+,MCF}}{D_{Li^+,BCF}} = \left(\frac{\sigma_{BCF}}{\sigma_{MCF}}\right)^2 \quad (3)$$

The surface modification of the current collector has increased the lithium-ion diffusion coefficient by about 56 % according to Equation (3). The higher lithium diffusion coefficient for the MCF anode can be attributed to this electrode tortuosity. The tortuosity can augment the conductivity of the electrolyte and the effective diffusion coefficient. The short distances of diffusion can be made across the electrode as the tortuosity decreases. It can yield an increase in the lithium diffusion coefficient.

Table 3. Simulation results obtained from impedance spectrum of BCF and MCF anodes

Sample	R_s (Ω)	R_{SEI} (Ω)	CPE_{SEI}		R_{ct} (Ω)	CPE_{ct}		W (mMho)
			Y_o (μMho)	N		Y_o (μMho)	N	
BCF	20.1	11.5	139	0.579	28.5	984	0.614	219
MCF	12.4	13.7	20.8	0.693	23.2	742	0.656	267

4. CONCLUSIONS

In the present study, a mechanical method was applied to surface modification of copper current collector to be used in the preparation of lithium-ion battery anodes. The general conclusions are as follows:

(1) Improvement of the mechanical properties of the modified anode was confirmed using the adhesion strength test.
(2) The electrochemical studies of BCF and MCF anodes showed that the initial discharge capacity of graphite anode coated on the MCF (323.6 mAh g^{-1}) was about 8 % higher than the BCF anode (299.9 mAh g^{-1}).
(3) The BCF anode capacity reached 227.9 mAh g^{-1} after 100 charge/discharge cycles at 0.5C rate, while this value was 247.7 mAh g^{-1} for MCF anode.

The results of electrochemical impedance spectra demonstrated that the diffusion coefficient of lithium ion for MCF anode was about 56 % higher than that for BCF anode. On the other hand, the surface modification of the copper current collector reduced the charge transfer resistance of anode from 28.5 Ω to 23.2 Ω.

5. ACKNOWLEDGEMENT

The authors would like to thank the Energy Storage Department of Institute of Mechanics for financial support.

REFERENCES

1. Moghim, M.H., Eqra, R., Babaiee, M., Zarei-Jelyani, M. and Loghavi, M. M., "Role of reduced graphene oxide as nano-electrocatalyst in carbon felt electrode of vanadium redox flow battery", ***Journal of Electroanalytical Chemistry***, Vol. 789, (2017), 67-75. (https://doi.org/10.1016/j.jelechem.2017.02.031).
2. Zarei-Jelyani, M., Rashid-Nadimi, S. and Asghari, S., "Treated carbon felt as electrode material in vanadium redox flow batteries: A study of the use of carbon nanotubes as electrocatalyst", ***Journal os Solid State Electrochemistry***, Vol. 21, (2017), 69-79. (https://doi.org/10.1007/s10008-016-3336-y).
3. Loghavi, M.M., Eqra, R. and Mohammadi-Manesh, H., "Preparation and characteristics of graphene/Y_2O_3/$LiNi_{0.8}Co_{0.15}Al_{0.05}O_2$ composite for the cathode of lithium-ion battery", ***Journal of Electroanalytical Chemistry***, Vol. 862, (2020), 113971. (https://doi.org/10.1016/j.jelechem.2020.113971).
4. Gholami, M., Zarei-jelyani, M., Babaiee, M., Baktashian, Sh. and Eqra, R., "Physical vapor deposition of TiO_2 nanoparticles on artificial graphite: An excellent anode for high rate and long cycle life lithium-ion batteries", ***Ionics***, Vol. 26, (2020), 4391-4399. (https://doi.org/10.1007/s11581-020-03579-5).
5. Zarei-Jelyani, M., Baktashian, Sh., Babaiee, M. and Eqra, R., "Improved mechanical and electrochemical properties of artificial graphite anode using water-based binders in lithium-ion batteries", ***Journal of Renewable Energy and Environment (JREE)***, Vol. 5, (2018), 34-39. (http://dx.doi.org/10.30501/jree.2018.93555).
6. Zarei-Jelyani, M., Sarshar, M., Babaiee, M. and Tashakor, N., "Development of lifetime prediction model of lithium-ion battery based on minimizing prediction errors of cycling and operational time degradation using genetic algorithm", ***Journal of Renewable Energy and Environment (JREE)***, Vol. 5, (2018), 60-63. (http://dx.doi.org/10.30501/jree.2018.93531).
7. Sarshar, M., Zarei-Jelyani, M. and Babaiee, M., "Application of semi empirical and multiphysics models in simulating lithium ion battery operation", ***Proceedings of the 10th International Chemical Engineering Congress and Exhibition***, Isfahan, Iran, (2018). (https://www.researchgate.net/publication/325010205_Application_of_semi_empirical_and_Multiphysics_models_in_simulating_lithium_ion_battery_operation), (Accessed: 29 November 2021).
8. Chen, J., Xu, Y., Cao, M., Zhu, C., Liu, X., Li, Y. and Zhong, S., "A stable 2D nano-columnar sandwich layered phthalocyanine negative electrode for lithium-ion batteries", ***Journal of Power Sources***, Vol. 426, (2019), 169-177. (https://doi.org/10.1016/j.jpowsour.2019.04.027).
9. Yan, K., Lee, H.W., Gao, T., Zheng, G., Yao, H., Wang, H. and Cui, Y., "Ultrathin two-dimensional atomic crystals as stable interfacial layer for improvement of lithium metal anode", ***Nano Letters***, Vol. 14, (2014), 6016-6022. (https://doi.org/10.1021/nl503125u).
10. Zhang, J., Liu, Z., Kong, Q., Zhang, C., Pang, S., Yue, L. and Cui, G., "Renewable and superior thermal-resistant cellulose-based composite nonwoven as lithium-ion battery separator", ***ACS Applied Materials & Interfaces***, Vol. 5, (2013), 128-134. (https://doi.org/10.1021/am302290n).
11. Chen, J., Zhang, Q., Zeng, M., Ding, N., Li, Z., Zhong, S. and Yang, G., "Carboxyl-conjugated phthalocyanines used as novel electrode materials with high specific capacity for lithium-ion batteries", ***Journal of Solid State Electrochemistry***, Vol. 20, (2016), 1285-1294. (https://doi.org/10.1007/s10008-016-3126-6).
12. Zhang, L., Liu, Z., Cui, G. and Chen, L., "Biomass-derived materials for electrochemical energy storages", ***Progress in Polymer Science***, Vol. 43, (2015), 136-164. (https://doi.org/10.1016/j.progpolymsci.2014.09.003).
13. Zhu, C., Chen, J., Liu, S., Cheng, B., Xu, Y., Zhang, P. and Zhong, S., "Improved electrochemical performance of bagasse and starch-modified $LiNi_{0.5}Mn_{0.3}Co_{0.2}O_2$ materials for lithium-ion batteries", ***Journal of Materials Science***, Vol. 53, (2018), 5242-5254. (https://doi.org/10.1007/s10853-017-1926-4).
14. Li, Y., Chen, X., Dolocan, A., Cui, Z., Xin, S., Xue, L. and Goodenough, J.B., "Garnet electrolyte with an ultralow interfacial resistance for Li-metal batteries", ***Journal of the American Chemical Society***, Vol. 140, (2018), 6448-6455. (https://doi.org/10.1021/jacs.8b03106).
15. Huang, B., Xu, B., Li, Y., Zhou, W., You, Y., Zhong, S. and Goodenough, J.B., "Li-ion conduction and stability of perovskite $Li_{3/8}Sr_{7/16}Hf_{1/4}Ta_{3/4}O_3$", ***ACS Applied Materials & Interfaces***, Vol. 8, (2016), 14552-14557. (https://doi.org/10.1021/acsami.6b03070).
16. Ji, J., Liu, J., Lai, L., Zhao, X., Zhen, Y., Lin, J. and Ruoff, R.S., "In situ activation of nitrogen-doped graphene anchored on graphite foam for a

high-capacity anode", ***ACS Nano***, Vol. 9, (2015), 8609-8616. (https://doi.org/10.1021/acsnano.5b03888).

17. Li, J., Zhang, Q., Xiao, X., Cheng, Y.T., Liang, C. and Dudney, N.J., "Unravelling the impact of reaction paths on mechanical degradation of intercalation cathodes for lithium-ion batteries", ***Journal of the American Chemical Society***, Vol. 137, (2015), 13732-13735. (https://doi.org/10.1021/jacs.5b06178).
18. Zuo, T.T., Wu, X.W., Yang, C.P., Yin, Y.X., Ye, H., Li, N.W. and Guo, Y.G., "Graphitized carbon fibers as multifunctional 3D current collectors for high areal capacity Li anodes", ***Advanced Materials***, Vol. 29, (2017), 1700389. (https://doi.org/10.1002/adma.201700389).
19. Shin, D.Y., Park, D.H. and Ahn, H.J., "Interface modification of an Al current collector for ultrafast lithium-ion batteries", ***Applied Surface Science***, Vol. 475, (2019), 519-523. (https://doi.org/10.1016/j.apsusc.2019.01.016).
20. Lu, L.L., Ge, J., Yang, J.N., Chen, S.M., Yao, H.B., Zhou, F. and Yu, S.H., "Free-standing copper nanowire network current collector for improving lithium anode performance", ***Nano Letters***, Vol. 16, (2016), 4431-4437. (https://doi.org/10.1021/acs.nanolett.6b01581).
21. Park, H., Um, J.H., Choi, H., Yoon, W.S., Sung, Y.E. and Choe, H., "Hierarchical micro-lamella-structured 3D porous copper current collector coated with tin for advanced lithium-ion batteries", ***Applied Surface Science***, Vol. 399, (2017), 132-138. (https://doi.org/10.1016/j.apsusc.2016.12.043).
22. Zhang, P., Ma, Z., Wang, Y., Zou, Y., Sun, L. and Lu, C., "Lithiation-induced interfacial failure of electrode-collector: A first-principles study", ***Materials Chemistry and Physics***, Vol. 222, (2019), 193-199. (https://doi.org/10.1016/j.matchemphys.2018.10.018).
23. Shu, J., Shui, M., Huang, F., Xu, D., Ren, Y., Hou, L. and Xu, J., "Comparative study on surface behaviors of copper current collector in electrolyte for lithium-ion batteries", ***Electrochimica Acta***, Vol. 56, (2011), 3006-3014. (https://doi.org/10.1016/j.electacta.2011.01.004).
24. Nara, H., Mukoyama, D., Shimizu, R., Momma, T. and Osaka, T., "Systematic analysis of interfacial resistance between the cathode layer and the current collector in lithium-ion batteries by electrochemical impedance spectroscopy", ***Journal of Power Sources***, Vol. 409, (2019), 139-147. (https://doi.org/10.1016/j.jpowsour.2018.09.014).
25. Wu, J., Zhu, Z., Zhang, H., Fu, H., Li, H., Wang, A. and Hu, Z., "Improved electrochemical performance of the silicon/graphite-tin composite anode material by modifying the surface morphology of the Cu current collector", ***Electrochimica Acta***, Vol. 146, (2014), 322-327. (https://doi.org/10.1016/j.electacta.2014.09.075).
26. Kang, S., Xie, H., Zhai, W., Ma, Z.F., Wang, R. and Zhang, W., "Enhancing performance of a lithium ion battery by optimizing the surface properties of the current collector", ***International Journal of Electrochemical Science***, Vol. 10, (2015), 2324-2335. (http://www.electrochemsci.org/papers/vol10/100302324.pdf), (Accessed: 29 November 2021).
27. Jeon, H., Cho, I., Jo, H., Kim, K., Ryou, M.H. and Lee, Y.M., "Highly rough copper current collector: improving adhesion property between a silicon electrode and current collector for flexible lithium-ion batteries", ***RSC Advances***, Vol. 7, (2017), 35681-35686. (https://doi.org/10.1039/C7RA04598K).
28. Jiang, J., Nie, P., Ding, B., Wu, W., Chang, Z., Wu, Y. and Zhang, X., "Effect of graphene modified Cu current collector on the performance of $Li_4Ti_5O_{12}$ anode for lithium-ion batteries", ***ACS Applied Materials & Interfaces***, Vol. 8, (2016), 30926-30932. (https://doi.org/10.1021/acsami.6b10038).
29. Zhang, N., Zheng, Y., Trifonova, A. and Pfleging, W., "Laser structured Cu foil for high-performance lithium-ion battery anodes", ***Journal of Applied Electrochemistry***, Vol. 47, (2017), 829-837. (https://doi.org/10.1007/s10800-017-1086-x).
30. Yoon, T., Chapman, N., Nguyen, C.C. and Lucht, B.L., "Electrochemical reactivity of polyimide and feasibility as a conductive binder for silicon negative electrodes", ***Journal of Materials Science***, Vol. 52, (2017), 3613-3621. (https://doi.org/10.1007/s10853-016-0442-2).
31. Mao, C., Wood, M., David, L., An, S.J., Sheng, Y., Du, Z., Meyer III, H.M., Ruther, R.E. and Wood III, D.L., "Selecting the best graphite for long-life, high-energy Li-ion batteries", ***Journal of The Electrochemical Society***, Vol. 165, No. 9, (2018), A1837-A1845. (https://iopscience.iop.org/article/10.1149/2.1111809jes/pdf), (Accessed: 29 November 2021).
32. Steinhauer, M., Risse, S., Wagner, N. and Friedrich, K.A., "Investigation of the solid electrolyte interphase formation at graphite anodes in lithium-ion batteries with electrochemical impedance spectroscopy", ***Electrochimica Acta***, Vol. 228, (2017), 652-658. (https://doi.org/10.1016/j.electacta.2017.01.128).
33. Zarei-Jelyani, M., Babaiee, M., Baktashian, Sh. and Eqra, R., "Unraveling the role of binder concentration on the electrochemical behavior of mesocarbon microbead anode in lithium–ion batteries: Understanding the formation of the solid electrolyte interphase", ***Journal of Solid State Electrochemistry***, Vol. 23, (2019), 2771-2783. (https://doi.org/10.1007/s10008-019-04381-8).